



Assessment of an auto-routing method for topology generation of aircraft power supply systems

Thimo Bielsky¹ · Nils Kuelper¹ · Frank Thielecke¹

Received: 27 February 2023 / Revised: 6 December 2023 / Accepted: 19 March 2024
© The Author(s) 2024

Abstract

During early phases of aircraft development, overall systems design is performed to estimate relevant system design parameters such as mass, power consumption, and compliance with architectural requirements (redundancy). The *GeneSys* software framework has been developed for parametric modeling of aircraft on-board systems for overall systems design. To this end, model-based architecture definition, topology generation (components positioning and connections routing), and system sizing are conducted. The topology generation is currently performed using design templates containing knowledge-based heuristics derived from systems topologies of existing aircraft. However, using such design templates limits their generic application to novel aircraft models because exceptions for geometric differences between these models need to be implemented. This especially applies to the topology generation of power supply systems (electric, hydraulic) due to their high number of interfaces to consumer systems. To overcome these limitations, an automated routing method is presented in this paper as a generic approach for topology generation. With this method, the system topology is generated based on a defined routing network, which comprises areas of the aircraft for allowed components positioning and connections routing. Using Dijkstra's algorithm, the shortest path connections are found within the established routing network. Furthermore, boundary conditions for routing, for instance adding a cost function for power segregation, can be defined. An assessment of the automated routing method applied on the electric power supply system is performed using qualitative parameters such as the capability to adapt the routing network. Quantitative parameters like cable length and system mass are assessed as well.

Keywords Overall systems design · Electric power supply system · Topology · Auto-routing

List of symbols

C	Cost function
D	Density of a graph
E	Number of edges in a graph
f	Total cost for shortest path finding
G	Graph
g	Cost from start node to current node

h	Heuristic to estimate cost from current node to target node
M	Set of nodes that are part of a path
n	Current node
p	Previous node
V	Number of nodes in a graph

Abbreviations

APPU	Asymmetry position pick-off unit
CP	Concept plane
CPACS	Common Parametric Aircraft Configuration Schema
DC	Direct current
DLR	German Aerospace Center
DSD	Detailed systems design
ECS	Environmental control system
EHA	Electro-hydrostatic actuator
EHSA	Electro-hydraulic servo actuator
EMA	Electro-mechanic actuator
EPSS	Electric power supply system

Nils Kuelper and Frank Thielecke have contributed equally to this work.

✉ Thimo Bielsky
t.bielsky@tuhh.de
Nils Kuelper
nils.kuelper@tuhh.de
Frank Thielecke
frank.thielecke@tuhh.de

¹ Institute of Aircraft Systems Engineering, Hamburg
University of Technology, Nesspriel 5, 21129 Hamburg,
Germany

ESBEF	Development of Systems and Components for Electrified Flight
FCS	Flight control system
FST	Institute of Aircraft Systems Engineering
HPP	Hydraulic power package
HTP	Horizontal tail plane
HVDC	High-voltage direct current
MEA	More electric aircraft
OAD	Overall aircraft design
OSD	Overall systems design
PCU	Power control unit
PEPDC	Primary electric power distribution center
PFCS	Primary flight control system
PMAD	Power management and distribution unit
SArA	Systems architecting assistant
SEPDC	Secondary electric power distribution center
SPDB	Secondary power distribution box
TLAR	Top-level aircraft requirement
TUHH	Hamburg University of Technology
VTP	Vertical tail plane
WTB	Wing tip brake

1 Introduction

In the initial stages of aircraft development, the process of overall systems design (OSD) is undertaken to ascertain optimal on-board systems designs tailored to a specific concept aircraft model. To this end, rapid concept studies are conducted by varying, for example, systems architectures (logical components and their interrelations) or systems topologies (component positioning and connection routing) [1]. For this purpose, high-fidelity models for OSD are required for higher certainty in the results of the concept studies.

The high-fidelity, physics-based *GeneSys* software framework for OSD has been developed by the Institute of Aircraft Systems Engineering (FST) at Hamburg University of Technology (TUHH) to perform such concept studies for aircraft on-board systems [1–5]. This OSD framework consists of different process steps such as systems architecture definition and systems sizing. The model fidelity for OSD has been increased with the *GeneSys* framework by performing the systems design based on geometric characteristics of the aircraft model using the systems topology. Currently, the systems topology is generated based on the geometry of the aircraft model and the defined systems architecture using knowledge-based design templates and heuristics.

However, the approach to generate the systems topology by knowledge-based design templates is limited due to the following aspects:

- Knowledge-based design templates are derived from existing aircraft and are consequently valid for existing aircraft only.
- Complex and time-consuming process for power supply systems with a high number of consumer systems, as each connection needs to be defined manually.
- These topology templates are inflexible as it is necessary to manually create alternative templates to account for various system topology variants.
- Adaptations of the topologies, such as considering minimum distances between systems, can only be performed manually.

In addition, the evaluation focus for on-board systems concept studies is currently primarily on mass and power requirements. The existing knowledge-based design templates face limitations in assessing other relevant factors like systems integration criteria. These criteria include segregation conditions, installation and maintenance aspects, and interdependencies between on-board systems. The current approach does not allow for a comprehensive evaluation of these aspects. To address the above described limitations, an alternative, more generic approach for topology generation is necessary to increase its flexibility and to decrease the workload for adaptations of the topology.

In this paper, an automated routing method is proposed and evaluated to overcome the limitations of the existing knowledge-based design templates. The automated routing method is applied to generate the topology of power supply and other network systems, such as hydrogen storage and distribution. This approach creates the possibility to generate the system topology based on a defined routing network, eliminating the need for manual definition of each connection. Moreover, boundary conditions such as power segregation, no-routing areas, and minimum distances to other on-board systems can be integrated due to the more generic approach by, for example, adding cost functions [6].

Furthermore, connections between systems are defined as the direct way between two components. Auxiliary components (joints) are defined for each connection to depict both the geometry of the aircraft model and the path of the cable within the aircraft. The higher the number of these joints, the better the cable routing is represented. However, a high number of joints requires an increased computing time for generating the systems topology. In addition, the computing time for systems sizing also increases because it is performed based on the generated topology. Therefore, the computing time is dependent on the number of the generated components and connections. Studies are conducted to assess the impact on the system by adapting such boundary conditions of the auto-routing method to determine the level of discretization required for the design.

The paper is structured as follows. The *GeneSys* framework for OSD is described in more detail in Sect. 2. In Sect. 3, the knowledge-based approach for topology generation in *GeneSys* is described. The auto-routing method is presented in Sect. 4, followed by Sect. 5, in which the application to the electric power supply system (EPSS) in a regional concept aircraft is presented.

2 Overall systems design framework

As part of aircraft conceptual design, abstraction levels of aircraft, system, and component models are considered [1, 2, 5]. From the perspective of a system engineer, these levels are overall aircraft design (OAD), systems architecting, OSD, and detailed systems design (DSD) [3], as shown in Fig. 1.

In general, the conceptual design process is initiated by defining geometric characteristics of the aircraft and top-level aircraft requirements (TLARs) as part of OAD [3]. Regression functions and statistical methods are used to initially estimate TLARs like flight altitude, payload, and range [1]. Requirements for OSD, such as secondary power demands, are directly derived from TLARs [7, 8]. To manage requirements and geometric information, the Common Parametric Aircraft Configuration Schema (CPACS) defined by the German Aerospace Center (DLR) [9] is providing a generic interface file between OAD and other conceptual design disciplines on a higher fidelity level [2].

To cope with the advancing maturity of on-board systems during aircraft development, system, subsystem, and component requirements need to be validated as part of

DSD [1]. Therefore, systems' behavior analysis based on transient simulations is performed. However, the development of these high-fidelity, time-dependent simulations is a time-consuming process, limiting detailed system analysis capabilities to few variants. Moreover, required data for DSD simulations, such as a previously defined systems architecture, are not provided by OAD [1]. To obtain the required data and to identify optimal systems designs, systems architectures need to be defined and rapid concept studies on OSD level need to be performed. Therefore, the general process as part of the OSD framework has been developed and is demonstrated in Fig. 2. The process includes five steps: pre-processing, systems architecting, topology generation, sizing and simulation, and post-processing [1].

Systems architecting as the second process step is performed using the *systems architecting assistant (SArA)* methodology [3]. *SArA* works as an integrated approach, assisting the engineer during the process of generating logical systems architecture variants, validation, evaluation, and selection [3]. In general, a logical system architecture describes a system based on its high-level, logical components and their interrelations to demonstrate how functions are realized. Furthermore, only a pre-selection of technology concepts without a particular physical component technology selection is included to enable an architecture definition independent of a particular detailed solution [3, 10].

Afterward, rapid concept studies are conducted using the *GeneSys* software framework to evaluate the effect of architecture variations on system and aircraft level [3]. *GeneSys* as part of OSD consists of several modules, such as topology generation and system sizing, which are shown in Fig. 2. The

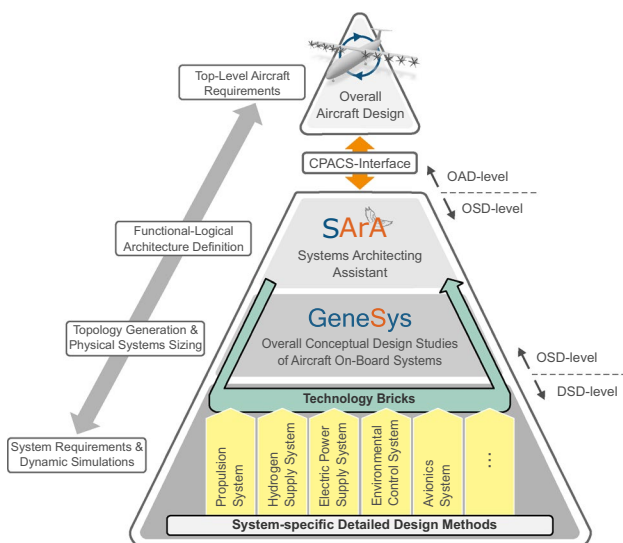


Fig. 1 Different levels and disciplines of conceptual aircraft design phase

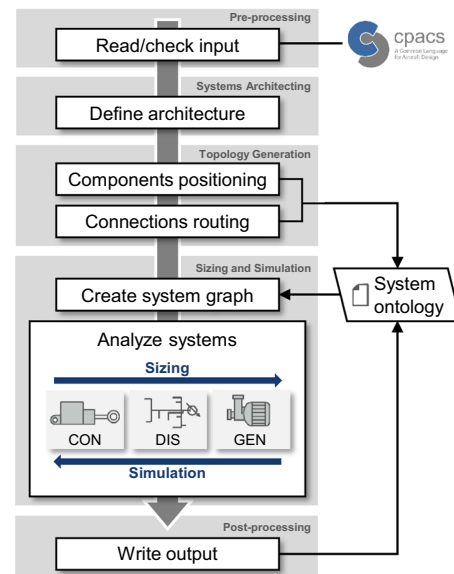


Fig. 2 Process diagram for OSD framework

generated systems topology can be visualized within *GeneSys* to visually verify component positioning and routing results. Based on systems topology as well as system-specific boundary conditions, parametric system sizing is performed taking into account static system simulations and technology functions. Furthermore, interdependencies between different on-board systems that might occur during the sizing process are considered [1, 5]. System sizing results, such as systems mass, power consumption, and total energy demand, are saved as parametric file as part of the post-processing step. Concept study results are used to rapidly conduct a comparison of systems architecture variants on OSD level.

To generate the systems topology based on the defined systems architecture while ensuring a seamless process chain during conceptual design, a parameter-based XML interface template, which considers design and architectural information, is employed [1, 3]. The interface file includes both metadata and characteristics of the defined systems architecture, such as logical system components, inputs and outputs, logical connections, and component properties.

3 Design templates and heuristics for systems topology generation

The generation of the systems topology is performed with generic design templates and heuristics based on existing aircraft models. These design templates are created based on the defined systems architecture and the geometry of the aircraft, which is defined in the CPACS file. Relevant information from the systems architecture are the number of components (e.g., pumps, generators) defined in each system, the power type (e.g., electric, hydraulic), which is used for power supply, and systems interconnections. Furthermore, relevant information from the CPACS file are geometric design characteristics that can be used as boundary conditions for generating the systems topology. Such design characteristics are, for example, the definition of spars in wing and tail planes and the definition of utilization areas (i.e., decks), such as cabin, cockpit, and cargo decks. The defined decks include further geometric definitions, for instance, seats, galleys, lavatories, aisles, and doors.

For the knowledge-based approach, the systems topologies of different existing aircraft models are analyzed. This includes the evaluation of their similarities and differences. A generic approach is developed to represent significant characteristics in the design template. However, specific characteristics, which may apply only to one aircraft model, are usually neglected in case they do not fit into a generic representation of the systems topology. Such deviations have to be compensated in the sizing laws of the particular system, which is used to perform the system sizing [1, 11]. In the following, examples of the environmental control system

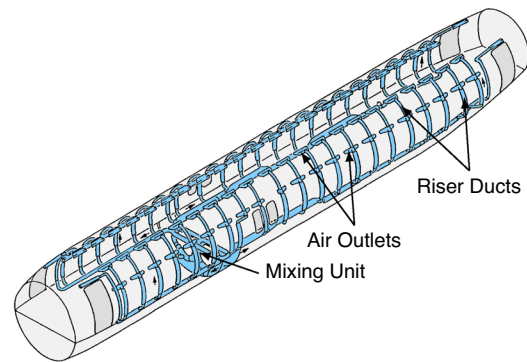


Fig. 3 System topology of the ECS in the *Airbus A320* [12]

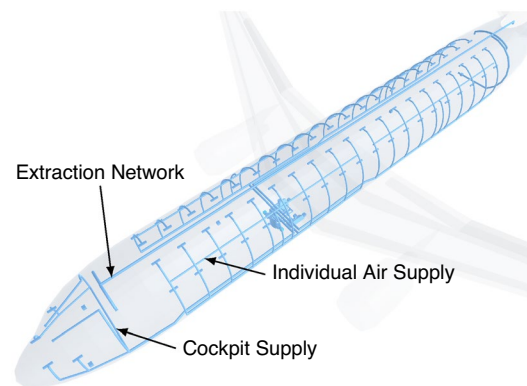


Fig. 4 ECS topology result using the knowledge-based design template in an *A320*-like aircraft model

(ECS) and the flight control system (FCS) are presented to further explicate the knowledge-based design templates.

In the example of the ECS, the cabin air distribution network of the *Airbus A320* as shown in Fig. 3 is presented. Air is supplied from the mixing unit through ducts, which are located on both sides near the fuselage wall and the cabin floor [12, 13]. From there, riser ducts go up to the cabin ceiling, supplying air to the cabin through air outlets. This topology variant of the *Airbus A320* is called *single riser ducts* [12]. The ECS topology generated by *GeneSys* for an *Airbus A320*-like aircraft model is shown in Fig. 4. Besides the cabin air supply, the cockpit supply, avionic fans, the individual air supply for passengers, and the air extraction network are also shown in here. To create the generic design template for generating the ECS topology, the main assumption is to equally distribute air outlets and riser ducts along the cabin deck. However, the riser ducts are located between the windows, which are not defined in the CPACS file. Hence, the number of windows per wing side of the aircraft model is required as further input for the ECS topology.

Another example is presented in the following, which shows the knowledge-based approach for the secondary flight control system (i.e., flap and slat drive systems). Figure 5 shows the secondary flight control system of the Airbus A320. Both flaps and slats are extended and retracted by a central drive system, which is driven by a power control unit (PCU). Each slat and each flap surface is driven by two actuators. A wing tip brake (WTB) is positioned before the last actuator of the shaft on each wing side to stop shaft movement in case an asymmetry is detected by the asymmetry position pick-off unit (APPU) due to a possible shaft break [13, 14]. The FCS topology generated by *GeneSys* for an Airbus A320-like aircraft model is displayed in Fig. 6. To position the shaft of the slat drive system, the wing front spar is used as reference, since it is also defined in the CPACS file. It is assumed that the shaft is positioned in front of the front spar. To position the shaft of the flap drive system, the leading edge definitions of the flaps are used as reference by the *GeneSys* design template. In comparison to Fig. 5, the flap PCU is positioned higher by the *GeneSys* design template for the A320-like aircraft model. The position of the flap PCU differs because its positioning is derived from data of different aircraft models to enable a generic positioning.

The generation of the routing network of the EPSS and other power supply systems is based on geometric design characteristics as well. As shown in Fig. 7, it is assumed for the EPSS that the main cable routes in the fuselage are defined to be placed along the crown area above the cabin, along the triangle areas, and along the cabin floor at the ceiling of the cargo deck. Main cable routes in the wing and tail planes are assumed to be located along their front and rear spars. These main cable routes are used in the knowledge-based approach as reference points for the design template to define a cable between each considered electrical consumer system and its connected power distribution component [e.g., primary electric power distribution center (PEPDC), secondary electric power distribution center (SEPD), or secondary power distribution box (SPDB)] [1, 3].

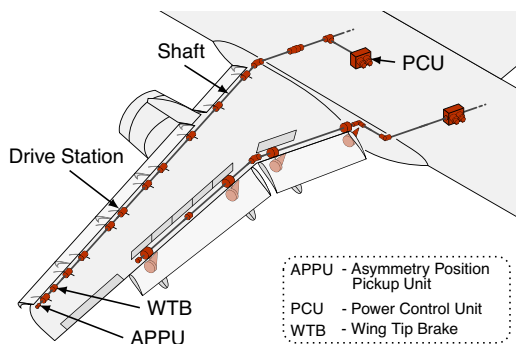


Fig. 5 System topology of the FCS in the Airbus A320 [14]

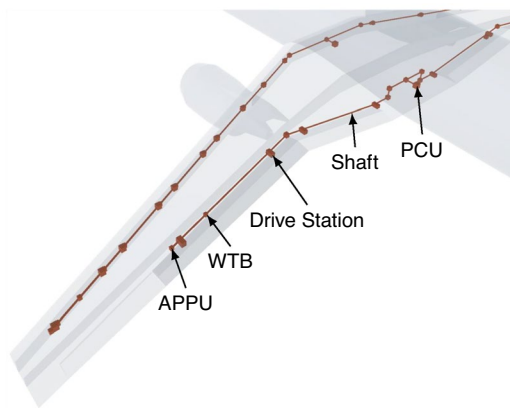


Fig. 6 FCS topology result using the knowledge-based design template in an A320-like aircraft model

4 Development of an automated routing method

The proposed auto-routing algorithm and its implementation is described in this section. First, an overview of relevant algorithms for finding the shortest path is presented. This also includes a more detailed explanation of the selected Dijkstra algorithm for shortest path finding. Second, the integration of the auto-routing algorithm in *GeneSys* is described. Last, adaptations of the algorithm to consider power segregation as boundary condition during topology generation are elaborated.

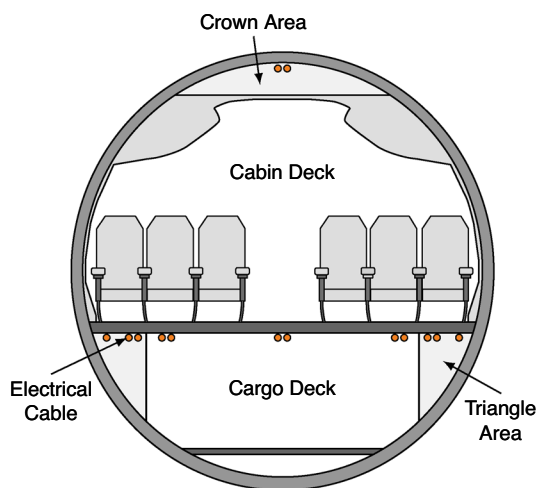


Fig. 7 Assumed routing paths of electrical cables in the fuselage of single-aisle aircraft

4.1 Overview of relevant routing algorithms

Applications for shortest path finding can be identified both in the personal environment and in industrial processes. Such path finding problems are usually based on graphs or grids. An industrial robot finding the shortest path in a 3D environment with several obstacles for assembling parts or the production of printed circuit boards is an example for applying path finding problems to grids [6, 15]. An example for applying the path finding problem to graphs are navigation systems [15].

Both graphs and grids can be used to apply the shortest path finding problem to the network of aircraft EPSS. To justify representing the network as a graph $G(V, E)$, where V is the number of nodes and E is the number of edges, or as a grid, the density D of undirected graphs is calculated using Eq. (1) [16]

$$D(V, E) = \frac{2 \cdot E}{V \cdot (V - 1)}. \quad (1)$$

A graph is considered as dense when its density is close to $D = 1$. In case of $D = 1$, all nodes are connected with each other. If the density value is close to $D = 0$, the graph is considered sparse [16, 17]. It is more suitable to represent dense graphs as a grid. In a sparse graph, fewer edges are connected with each other, leading to a significantly increased size of the grid.

Since the auto-routing algorithm is performed on OSD level, only cables with significant impact on the system design are considered [1]. Therefore, typical routing areas are identified and selected for generating the systems topology. These aspects are based on geometrical characteristics of the aircraft (cf. Sect. 3). Section 5.1.3 shows the integration of the auto-routing method for the EPSS to a hydrogen-powered concept aircraft. In this example, the graph of the EPSS routing network consists of $V = 449$ nodes and $E = 471$ edges (cf. Fig. 13), assuming a maximum distance between nodes of 1.25 m (cf. Sect. 5.2.2). Using Eq. (1), the density of this graph is calculated as $D = 0.005$, indicating a sparse graph. Thus, the graph representation of the EPSS is more suitable for this particular routing problem. In contrast, a grid representation of the aircraft for cable routing would be more suitable for detailed systems design, considering all power and signal cables as well as their attachment points in the 3D environment for installation [6, 15, 18].

A simplified example of an undirected graph is shown in Fig. 8 to represent the path finding problem. The graph shown in Fig. 8 has 6 nodes (A, \dots, F) and 7 edges connecting the nodes with each other. Each edge is weighted, which represents its distance between the connecting nodes. In this simplified example, the shortest path

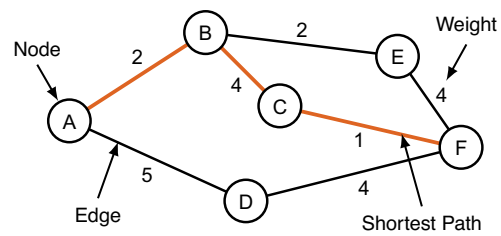


Fig. 8 Example of a simplified graph with highlighted shortest path between node A and node F

between nodes A and F can be manually determined as $A - B - C - F$ with the total distance of $f_{ABCF}(F) = 7$ [19].

To find the shortest path for cable routing within a graph, routing algorithms are employed. As the complexity of the graph increases (i.e., high number of nodes and edges), optimized routing algorithms are crucial for efficiently determining the shortest path. Common examples of algorithms for shortest path finding include Dijkstra's algorithm [20, 21], A^* algorithm [19], Bellman–Ford algorithm [20], and Floyd–Warshall algorithm [20]. Dijkstra's algorithm and the A^* algorithm are suitable for graphs with non-negative edge weights. These algorithms are used, for example, as an algorithm for navigation systems in video games [19]. In addition, Dijkstra's algorithm is also used in the tool *Pacelab SysArc* for system topology generation in aircraft conceptual design [22]. The Bellman–Ford algorithm is capable of handling graphs with negative edge weights, but it does not offer significant advantages over Dijkstra's algorithm or A^* algorithm. Finally, the Floyd–Warshall algorithm is less efficient compared to the other algorithms because the shortest paths between all nodes of the graph are calculated. Hence, the Bellman–Ford and Floyd–Warshall algorithms are not considered further for the pathfinding problem in this paper.

Using the example graph in Fig. 8, the A^* algorithm is described by Eq. (2) with the parameters g for the distance from the start node A to the current node n and h for a heuristic to estimate the remaining distance to the target node F . One possibility to determine the heuristic is to calculate the Euclidean distance between the current node n and the final node F [18]. This, however, requires that the coordinates of all nodes are known. For shortest path finding, the minimum of the function f at each node n is pursued [19]

$$f(n) = g(n) + h(n). \quad (2)$$

Dijkstra's algorithm can be described as a simplification of the A^* algorithm by neglecting the heuristic with $h(n) = 0$. In this case, Eq. (2) is written as $f(n) = g(n)$. Compared to the A^* algorithm, less information for finding the shortest path are required, but in many cases, more potential paths of the

graph have to be assessed to find the shortest path. This leads to an increased computing time. However, it is expected that the advantage of using the heuristic diminishes when the graph has a lower branching factor and is considered sparse. As described above, this applies to the graph representing the EPSS on OSD level. Therefore, Dijkstra’s algorithm is used for shortest path finding as part of the automated routing method.

In the following, the process of Dijkstra’s algorithm for finding the shortest path is explained in more detail. As an example, the shortest path between the nodes *A* and *F* of the graph in Fig. 8 is used. Table 1 lists the iterations of the Dijkstra algorithm to find the shortest path [20].

The first step is to visit the start node *A*. As this is the initial node, the cost (i.e., distance) is set to $f_A(A) = 0$. The distances to all other unvisited nodes are initially set to infinity. After visiting the start node *A*, its connected nodes *B* and *D* are analyzed in the second step. In this example, the distances are $f_{AB}(B) = 2$ and $f_{AD}(D) = 5$. As a greedy algorithm, Dijkstra selects the node with the lowest distance to proceed [20]. Therefore, node *B* is visited and its connected nodes *C* and *E* are analyzed in the third step. The distances are calculated to $f_{ABC}(C) = 6$ and $f_{ABE}(E) = 4$. Subsequently, node *E* is visited and its connections are analyzed in the fourth step. Node *E* is only connected to the target node *F* with a total distance of $f_{ABEF}(F) = 8$. However, even though the target node *F* is reached, the nodes *C* and *D* are still unvisited, meaning that a shorter path can exist. Thus, node *D* is visited next due to its lower distance compared to node *C*. In the fifth step, node *D* is analyzed and it is found to be connected to the target node *F* with a total distance of $f_{ADF}(F) = 9$. In this case, the path *A – B – E – F* is still preferred due to the lower distance. Lastly, node *C* is analyzed in the sixth step and the total distance is calculated to $f_{ABCF}(F) = 7$, which is lower than the previously calculated values. Consequently, all nodes have been visited and the

shortest path *A – B – C – F* is identified by retracing the table using information of the previously visited nodes.

4.2 Methodical integration into the OSD framework

As described before, a graph has to be created for the EPSS topology generation to apply an algorithm for shortest path finding. A simplified example of connecting routing areas to create a graph is shown in Fig. 9.

The first step is to define routing areas in which cable routing is possible. These routing areas are defined based on geometrical characteristics of the aircraft, which are, for example, along the front and rear spar of the wing, underneath the cabin floor, or above the cabin ceiling (cf. Fig. 7). For each routing area, several joints are defined. These joints are connected with each other, creating an area for allowed cable routing. In addition, these joints also fulfill the following purposes:

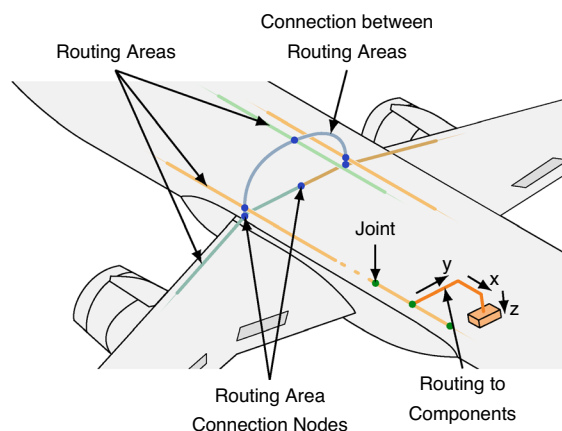


Fig. 9 Main routing areas and routing to consumer systems

Table 1 Example of Dijkstra’s algorithm to find the shortest path between nodes *A* and *F* in Fig. 8

Step		A	B	C	D	E	F	Unvisited nodes
1	Shortest dist. from A	0	∞	∞	∞	∞	∞	[A, B, C, D, E, F]
	Previous node	–	–	–	–	–	–	
2	Shortest dist. from A	0	2	∞	5	∞	∞	[B, C, D, E, F]
	Previous node	–	A	–	A	–	–	
3	Shortest dist. from A	0	2	6	5	4	∞	[C, D, E, F]
	Previous node	–	A	B	A	B	–	
4	Shortest dist. from A	0	2	6	5	4	8	[C, D, F]
	Previous node	–	A	B	A	B	E	
5	Shortest dist. from A	0	2	6	5	4	8	[C, F]
	Previous node	–	A	B	A	B	E	
6	Shortest dist. from A	0	2	6	5	4	7	[F]
	Previous node	–	A	B	A	B	C	

- Adaption of routing area to the geometrical characteristics of the aircraft because only direct connections between two joints can be defined.
- Point of access to the routing area for cable routing to components that are positioned nearby.

Hence, the number of joints affects how well a routing area can represent the actual system topology.

To obtain a single graph, all these defined routing areas have to be connected to each other. For this purpose, routing area connection nodes are defined in a second step. These connection nodes are placed in each routing area at possible intersection points with other routing areas. These are, among others, the intersection between the wing and the fuselage and the intersection between the wing and pylons for propulsion units. Furthermore, other geometrical boundary conditions are also considered for defining such connection nodes. These are, for instance, the beginning and the end of the cabin or the outboard side of the wing to possibly connect the routing areas along the front and rear spar with each other.

After all relevant connection nodes are identified according to geometrical boundary conditions and defined routing areas, the connection nodes of each interface group are connected with each other. The example in Fig. 9 shows that the defined routing areas of the wing are connected with all three routing areas of the fuselage.

Having obtained a single graph, the routing between components can be performed. For each routing, the definition of a start and a target component is required. As described above, the joint of the routing area that is positioned closest to the start component is identified. This also applies to the joint, which is positioned closest to the target component. The shortest path routing is performed between these two joints. Furthermore, boundary conditions are defined for routing between the components and its closest joint in the graph for better representation of the actual system topology. These boundary conditions depend on the position of the component within the aircraft. In Fig. 9, an example is shown for a component located underneath the cabin floor. In this case, a cable is routed first to the y -coordinate of the component, second to the x -coordinate of the component, and last to the component itself, covering the translation in z -direction.

4.3 Consideration of power segregation conditions

With the created graph that represents the possible routing network of the EPSS, further boundary conditions can be defined for the routing (e.g., segregation, consideration of no-routing areas, or minimum distance between different systems). In the scope of this paper, the boundary condition for segregation is further described. In case several flight

critical components fulfilling similar functions are located closely to each other, segregation of power supply needs to be performed (also for different power types) to avoid a single point of failure for this particular function due to a common cause error [13].

Figure 10 shows an example for segregation by applying a cost function $C = 2$. In this example, the shortest path between the nodes A and F is searched first as it is shown in Fig. 8. The distance of this path is $f_{ABCF}(F) = 7$. All nodes of the graph, which are part of this path, are assigned to the set $M = \{A, B, C, F\}$. Next, the nodes B and F shall be connected while considering the segregation constraint. According to Fig. 8, the shortest path between these nodes has a distance of $f_{BCF}(F) = 5$. However, due to the segregation constraint, a cost function of $C = 2$ is added. As described in Eq. (3), the value of the cost function C is multiplied to the initial cost of the edge of the graph, in case the current node n and the previous node p of the analyzed edge are both part of the set M . After applying the cost function, the shortest path between the nodes B and F is $B - E - F$ and has a distance of $f_{BEF}(F) = 6$.

$$f_{1,\dots,p,n}(n) = \begin{cases} g(n) \cdot C, & n \in M \wedge p \in M \\ g(n), & n \notin M \vee p \notin M \end{cases} \quad (3)$$

For the integration of the segregation constraint in the automated routing method, groups of system components, which require power segregation, need to be identified based on the defined systems architecture. The first component in such a group is defined as the one with the shortest Euclidean distance from the starting component of the routing. The path for this component is calculated using the Dijkstra algorithm without considering further boundary conditions. For all other components in this group, a cost function is applied to artificially increase the costs (or distances) of the edges that are part of the path to the first component. Other edges are not affected by this cost function (cf. Eq. (3)). A compromise needs to be identified for the value of the applied cost function, balancing between finding the shortest path for all components of a group and the shared use of the same path segments (i.e., overlap).

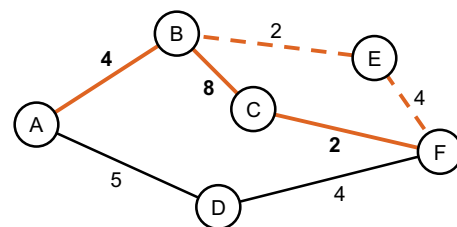


Fig. 10 Example for segregation using a cost function $C = 2$ (cf. Fig. 8)

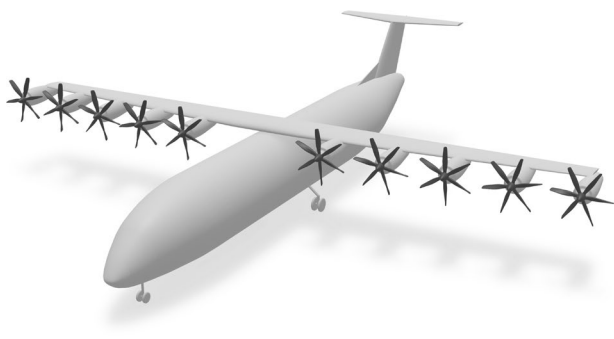


Fig. 11 Hydrogen-powered concept aircraft—*ESBEF-CPI*

Table 2 TLARs of the reference aircraft model

Characteristic	Value
Design range [NM]	1000
Cruise speed [–]	0.55
Cruise altitude [ft]	27,000
Max. PAX number [–]	70

5 Application to the EPSS of a hydrogen-powered concept aircraft

The application of the auto-routing algorithm to the EPSS of a hydrogen-powered concept aircraft is presented in the following. First, the problem set-up is defined including the description of the aircraft model and its systems architecture. Second, the auto-routing algorithm is assessed based on computing time and sensitivity studies. Last, power segregation is performed using the FCS as use case. Boundary conditions for segregation are assessed based on sensitivity studies.

5.1 Problem set-up

The reference aircraft model and its systems architecture, which are defined as reference for the assessment, are described in the following. This includes the application of the auto-routing algorithm to the EPSS with shortest path routing to all electrical consumer systems.

5.1.1 Reference aircraft model

The proposed auto-routing algorithm is assessed on the reference aircraft model. The name of the aircraft model is *ESBEF* (German acronym for *Development of Systems and Components for Electrified Flight*) Concept Plane 1 (CP1)

and is shown in Fig. 11 [3]. Table 2 lists the TLARs for the *ESBEF-CPI*.

The *ESBEF-CPI* is a regional hydrogen-powered concept aircraft based on an *ATR 72*-like aircraft platform. The *ESBEF-CPI* has ten propulsion units (i.e., pods), each containing fuel cell systems and their peripheral systems such as thermal management and air supply [3]. Each pod also includes a power management and distribution unit (PMAD) to control and distribute primary power supply (propulsion system) and secondary power supply (EPSS). Hydrogen storage is realized by two cryogenic tanks positioned in the aft fuselage. To maintain the same seating capacity as an *ATR 72*, the cabin configuration of the *ESBEF-CPI* has been adapted to a five-abreast seating configuration to shorten the cabin and allowing the integration of the cryogenic tanks. The systems architecture of the *ESBEF-CPI* follows a More Electric Aircraft (MEA) approach. Hence, the majority of the aircraft on-board systems are electrically powered, including an electric environmental control system, an electric de-icing system, and an electrically powered hydraulic power package (HPP) [3].

5.1.2 Considered systems architecture

In this paper, the focus is set on the EPSS and its consumer systems. It is assumed that the primary flight control system (PFCS) of the *ESBEF-CPI* is mainly supplied by electric power due to the MEA approach. As a safety critical consumer system of the EPSS, geometric segregation of electrical cable routing has to be considered to comply with safety requirements [13]. Thus, the PFCS is exemplarily considered in further detail as follows.

As shown in Fig. 12, the PFCS architecture includes hydraulic and electric actuators, and therefore requires both hydraulic and electric power supply. One actuator type used in this architecture is the electro-hydraulic servo actuator (EHSA). These actuators are supplied by a central HPP, which is located in the fuselage [4]. Since EHSA are as part of the PFCS considered as safety critical consumer systems, the HPP is supplied by both electric networks E1 and E2. However, since the focus of this paper lies on the EPSS architecture, EHSAs are shown only for completeness.

While EHSAs are centrally supplied by hydraulic power, electro-hydrostatic actuators (EHAs) are directly supplied by electric power of either network E1 or E2. EHAs are positioned at the ailerons, elevators, and rudder to actuate these surfaces. To accomplish that, electric power drives a hydraulic pump, powering a self-contained, local hydraulic network within the EHA [13, 23]. In contrast, an electro-mechanic actuator (EMA) performs a mechanical-based control surface actuation supplied by electric power without the integration of a local hydraulic system. Therefore, EMAs include an electric motor, a

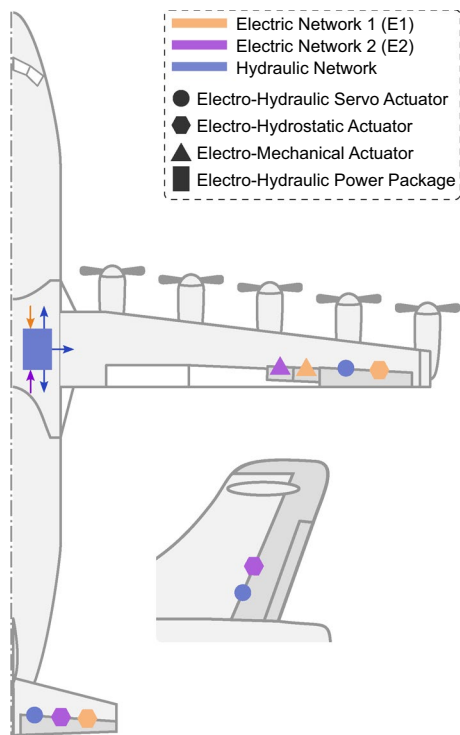


Fig. 12 Electrified primary flight control system architecture of *ESBEF-CPI*

gear, and a jack screw. Within the PFCS architecture of the *ESBEF-CPI*, EMAs are only used to actuate spoilers due to risk of mechanical jamming of the jack screw [13, 23].

Besides the shown electrified PFCS in Fig. 12, further electric-powered consumer systems relevant for OSD need to be considered for topology generation. These systems

are, among others, the electric environmental control system, cabin systems (e.g., lavatories, galleys), hydrogen infrastructure, electric de-icing, lights, and avionics.

5.1.3 Definition of the auto-routing network

The generation of the EPSS topology is performed based on defined routing areas. The routing areas that are defined for assessment are listed in the following:

- Triangle area left and right.
- Crown area.
- Wing front and rear spar.
- Propulsion units.
- Horizontal tail plane (HTP) front and rear spar.
- Vertical tail plane (VTP) front and rear spar.

In Fig. 13, the defined routing areas are visualized in the *ESBEF-CPI* aircraft model. In addition, the connection between routing areas in the fuselage are defined according to the following geometric boundary conditions: transition from cockpit to cabin deck, interface with wing front and rear spar routing areas, end of cabin deck, and interface with VTP front and rear spar routing areas.

In Fig. 14, the EPSS topology is visualized. Cables are routed based on the defined routing network between the PMADs and distribution units as well as between distribution units and all electrical consumer systems defined in Sect. 5.1.2 [3]. The routing itself is performed with the shortest path finding using Dijkstra's algorithm without considering further boundary conditions (cf. Sect. 4.1).

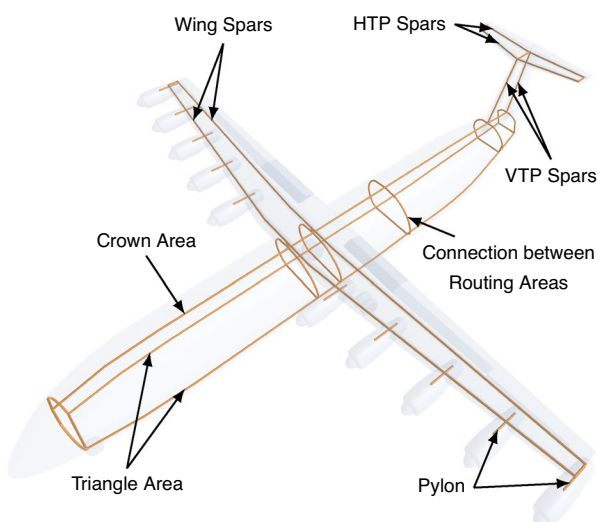


Fig. 13 Defined routing areas for the EPSS

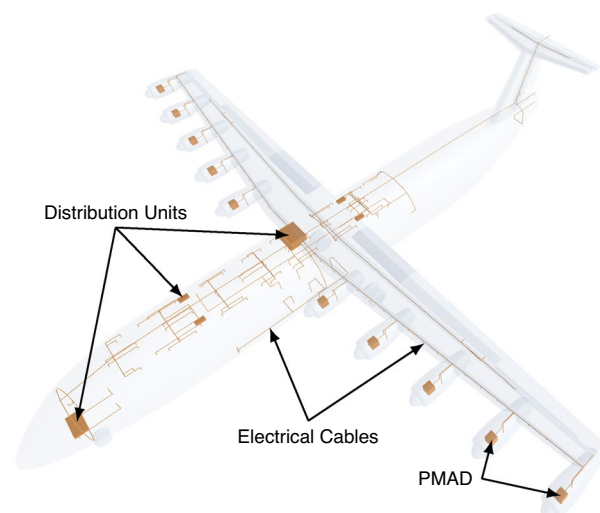


Fig. 14 Topology of the EPSS with shortest path routing

5.2 Assessment of the integrated auto-routing method

In the following, the auto-routing method is assessed. First, the auto-routing method is qualitatively compared to the knowledge-based template for generating EPSS topology in *GeneSys*. Second, boundary conditions of the auto-routing method, such as the number of joints of each routing area, are varied and the impact on the system design is assessed.

5.2.1 Qualitative comparison to the knowledge-based approach

Compared to the knowledge-based design template for EPSS topology generation, the auto-routing method has significant advantages. The main advantage of the auto-routing method is the flexibility of the generic definition of the routing areas. Defined routing areas can be added to or removed from the network by adapting the input file of the topology generation module in *GeneSys*. In case new routing areas have to be defined, which, for example, might be the case for a disruptive aircraft configuration, geometric characteristics of the new routing area and possible intersections to other routing areas (for defining connection nodes) need to be identified. Consequently, new routing areas are integrated into the graph to perform the shortest path finding.

In the knowledge-based design template, cable routing to each consumer system has to be manually defined, whereas consumer systems can be added without further adaptations using the auto-routing design template in *GeneSys* because cable routing is based on the generated routing graph. This also applies to different aircraft configurations such as low-wing, high-wing, or propulsion systems connected to the fuselage instead of the wing. In the knowledge-based design template, exceptions for every cable routing have to be manually implemented when adapting the design template for each possible aircraft configuration.

Furthermore, the auto-routing method creates the possibility to consider boundary conditions during topology generation. These include, among others, the abovementioned power segregation, restrictions in installation spaces like no-routing areas, or interdependencies between on-board systems.

One drawback of the auto-routing method is the increased computing time. Joints and connections of the routing networks are defined, which may not be used for the final routing. However, this effect is neglectable because the number of topology studies that are performed in *GeneSys* during conceptual design process for an aircraft model is rather low [1, 3].

5.2.2 Variation of the distance between the joints of the routing network

Relevant boundary conditions of the routing network can be adapted to assess its influence on EPSS sizing. One such boundary condition is the variation of the maximum distance between the joints of the routing network to determine the level of discretization required for the system design (cf. Sect. 4.2). The distance between the joints of the routing network represents the accessibility of the graph to perform the shortest path routing between two components. If the distance between joints increases, the routing distance from the component to its closest joint of the routing network may also increase. It could be the case that, at first, the routing is even performed in the opposite direction of the target component if that joint of the routing network is closest to the start component. Thus, it is assumed that an increase of the distance between joints leads to an increase of system mass and cable length.

The mass of the EPSS is calculated using *GeneSys* [1], employing a parametric approach to propagate relevant system parameters, such as electric power requirements and voltage level, from the electrical consumer systems through the network to the power sources. Thus, cables, distribution units (including converters and power controllers), and power sources are sized, considering losses within the electrical network, such as efficiencies and voltage drops within the cables [1, 5]. The main power specification of the EPSS of the *ESBEF-CPI* is high-voltage direct current (HVDC) at 270 VDC. In addition, there is availability of 28 VDC and local three-phase alternating current [5]. The design of the cables is conducted based on voltage drop criteria [1] and selected from the *Nexans* cable database [24]. For 270 VDC, cables can be selected from the *ABS 0949* catalog, for example. The mass of EPSS components, such as voltage transformers, is calculated based on a power-to-weight ratio. Relevant components and values for mass calculation are listed in Table 3 [5].

The EPSS mass and cable length are shown in Fig. 15 as a function of the distance between joints. As it can be seen, the initial assumption is verified. An adaption of the distance between joints from 0.1 to 5.0 m leads to an increase of the system mass by about 4 kg. However, the influence

Table 3 Values for mass calculation of relevant EPSS components for 2040

Component	Value	Source
Lithium-based battery	500 Wh/kg	[25]
Inverter	6.49 kW/kg	[26]
Solid-state power controller	30 kW/kg	[27]
DC/DC converter	25 kW/kg	[25]

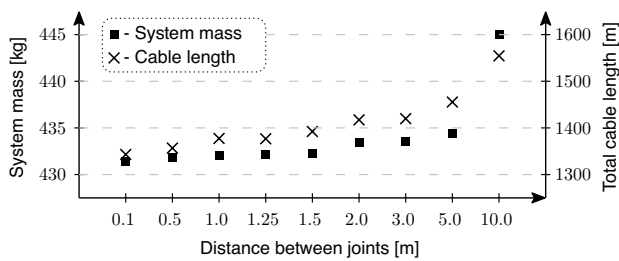


Fig. 15 EPSS mass and cable length as a function of the distance between the joints of the routing network

on the increase of the system mass is less than 1% compared to its total mass. This mass increase is neglectable for OSD [1, 11]. In contrast, the influence on the cable length is higher when further increasing the distance between joints. An increase of the distance between joints from 5.0 to 10.0 m leads to an increase of the system mass by about 11 kg. Due to the comparably significant mass increase, this variant is excluded from further evaluation.

Aside from that, decreasing the distance between joints has an increasing effect on the computing time because more joints and connections between the joints need to be defined. This effect is significant for a distance between joints of 0.5 m and 0.1 m.

In the scope of this study, a distance between joints of 1.25 m is selected as a best compromise between all considered parameters. However, since the influence on the system mass is not significant, the selection of other distances in the scope between 1.0 and 5.0 m is reasonable as well.

Applying the selected distance between joints to other aircraft geometries may still hold true when considering a suitable discretization of the system network. The mass deviation in Fig. 15 is mainly driven by the connections between the EPSS components and the joints for accessing the routing network. However, when, for instance, considering a larger aircraft, the relative system mass deviation decreases. Moreover, the computing time may become more relevant for larger aircraft, as more components and connections need to be created. In this case, the distance between joints should be increased incrementally.

5.3 Assessment of power segregation conditions

As it has been introduced in Sect. 4.3, power segregation is performed by defining groups of components whose power supply shall be segregated. A cost is added to the paths that are assigned to components of the same group to artificially increase the distance of the paths. Because the alternatively selected paths are not the shortest paths possible, it is assumed that an increase of the cost leads to an increase of

the cable length with simultaneously decreasing the number of shared path segments (i.e., overlap) of cables connected to components in one particular group. In the following, a group specific value for the cost function is determined to both minimize the overlap and minimize the increase of cable length.

Components defined in the same group for power segregation share in most cases the same path segments when applying the shortest path routing without defining further boundary conditions (cost function is set to $C = 1$). To calculate the overlap, a reference component needs to be defined. The reference is the target component that is located closest to the start component, i.e., has the shortest cable distance of all components in the particular segregation group. In this case, the overlap of all components in one segregation group is 100%. At a certain cost value, the artificial increase of the shortest path length exceeds the length of an alternative path. In this case, the overlap is reduced, but the cable length is increased. If the overlap is 0%, the alternative path does not share any path segments with the shortest reference path of a segregation group. However, it is possible that alternative paths cross the shortest path at an intersection point of the routing network. So far, this issue is neglected for the assessment but will be further discussed at the end of this section.

In the following, the cost is determined for two defined segregation groups of the *ESBEF-CPI* PFCS (cf. Fig. 12). The segregation groups are defined by location of the components, function of the components, and network of power supply. Group 1 includes the actuators of the right wing, which are connected to the electric network 1 (E1):

- Outer spoiler actuator right.
- Outer aileron actuator right.

Group 2 includes the actuators of the tail, which are connected to the electric network 2 (E2):

- Lower rudder actuator.
- Mid-elevator actuator right.
- Mid-elevator actuator left.

In Group 1, the shortest path between the PEPDC of the EPSS to the actuators in the wing is along the rear spar routing area of the wing (cf. Fig. 18). Since the spoiler actuator is located closer to the PEPDC, the shortest path between the PEPDC and the spoiler actuator is the reference for determining the overlap. To perform power segregation for this group, the cost is increased as shown in Fig. 16. As it can be seen, the overlap of the routing to the aileron actuator is 100% until the cost value reaches $C = 2.5$, meaning that both the cables to the spoiler actuator and to the aileron actuator share the rear spar routing area. At a cost of $C = 2.5$, the overlap drops to 0% and the cable length of this segregation

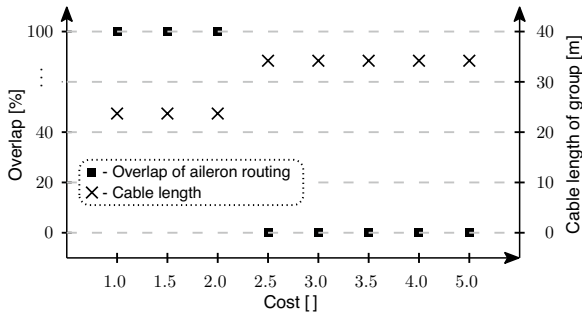


Fig. 16 Overlap and cable length of Group 1 as a function of the cost

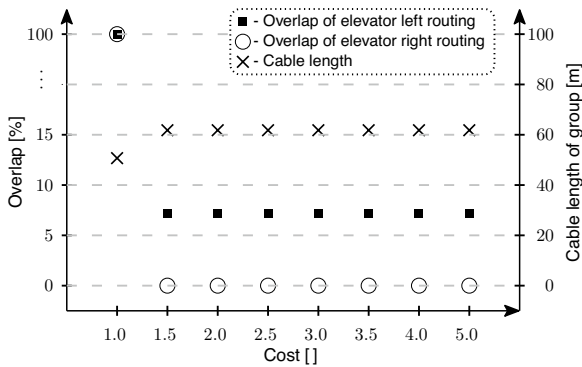


Fig. 17 Overlap and cable length of Group 2 as a function of the cost

groups increases by about 10 m. Hence, an alternative path is selected for the cable routing to the aileron actuator. As shown in Fig. 18, the cable to the aileron actuator is routed along the front spar of the wing.

Since the *ESBEF-CPI* has a t-tail, the shortest path between the PEPDC and the actuators of Group 2 is determined by the rudder actuator. In this case, the cable is routed along the crown routing area (cf. Fig. 18). A cost value of $C = 1.5$ leads to the selection of alternative paths for routing to the mid-elevator actuators (cf. Fig. 17). While the overlap of the routing to the right mid-elevator actuator drops to 0%, the overlap of the routing to the left mid-elevator actuator drops to about 7%. In this case, the cable length of Group 2 is increased by about 10 m. As shown in Fig. 18, the routing to the right mid-elevator actuator is performed along the right triangle area and along the front spar of the VTP. The routing to the left mid-elevator actuator is performed along the left triangle area and along the rear spar of the VTP. A further increase in the cost does not lead to a further drop in the overlap of the routing to the left mid-elevator actuator because shared routing areas cannot be avoided within the VTP with the routing network presented in Fig. 13.

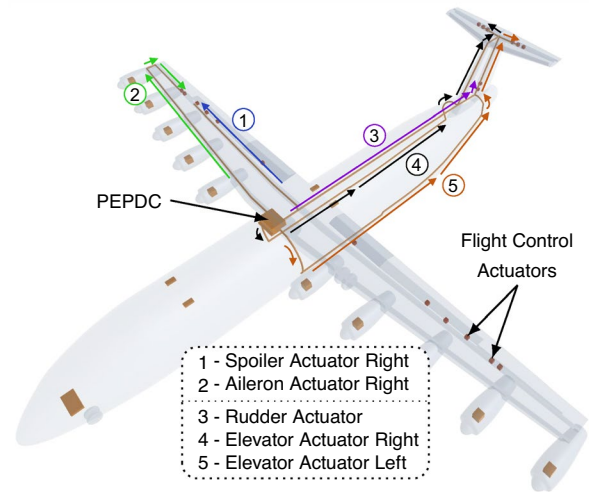
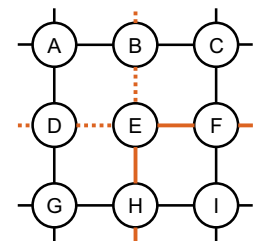


Fig. 18 Example for power segregation using selected cost functions ($C_{Group 1} = 2.5$ and $C_{Group 2} = 1.5$)

Fig. 19 Example of a graph with paths crossing at the same node despite segregated routing



Nevertheless, the overlap can be reduced to 0% by defining additional routing areas. For instance, multiple routing areas can be designated for the crown area, positioned next to each other. In addition, as illustrated in Fig. 7, additional routing areas can be defined at the ceiling of the cargo deck. Moreover, along the spars in the wings and tail planes, multiple routing areas can be defined. For example, these routing areas can be designated on both sides of the spar, either on the lower or upper side. With such a routing network, enough segregation paths can be found to eliminate the overlap in Group 2.

The selected values for the cost functions of the two segregation groups may differ for other aircraft models. The value depends on the geometry of the aircraft, on the position of the components (here acutators), and on the aircraft architecture. For example, the value of the cost function differs in case the aircraft has a conventional tail instead of a t-tail. Hence, the value for the cost functions for such segregation groups needs to be determined for each aircraft model.

As mentioned above, alternative paths may cross the shortest path at intersection points of the network. This

can be seen at the transition from the fuselage to the VTP of the *ESBEF-CPI* in Fig. 18. Figure 19 presents a simplified illustration of this issue. For example, the shortest path is routed along the nodes $F - E - H$ and another routing is performed along the nodes $B - E - D$ due to an applied segregation condition. In this case, both paths still meet in node E . To tackle this issue, it is proposed to add the cost function for segregation not only to the edges of the paths, but also to all edges that are connected to the nodes, which are part of the set M , hence which are part of the path. In this case, the segregated path is routed along $B - A - D$ instead of $B - E - D$. This approach may also be applied to the boundary condition for no-routing areas to avoid routing through specific installation spaces.

In addition to evaluating the overlap and the increase of cable lengths for power segregation, other key performance indicators must also be introduced to identify possible difficulties (e.g., for production or complying with regulations) during the routing process. First, the geometric distance between cable routes needs to be assessed. A cost function leads to the use of alternative paths, but such paths can still be located closely to the shortest reference path. This especially applies when more routing areas are defined that are positioned next to each other. Second, the time and effort in production for longer cable routings need to be evaluated for estimating the impact on production and maintenance cost. Last, available installation space and the assembly of the cable routings themselves in these spaces need to be assessed as well.

6 Summary and conclusion

The integration of an automated routing algorithm in the overall systems design software framework *GeneSys* for systems topology generation has been presented in this paper. According to the process steps of performing overall systems design using the *GeneSys* framework, systems topology is generated based on a beforehand defined systems architecture and geometric information of the aircraft model. The geometric information of the aircraft on-board systems, which are derived from the systems topology, are used for systems sizing and simulation. So far, knowledge-based design templates derived from existing aircraft are used to generate the systems topology. However, these design templates are inflexible and need to be manually adapted for compatibility to different aircraft configurations. To overcome these limitations of the existing knowledge-based design templates, a more generic approach is required for topology generation. Furthermore, evaluation criteria for systems topology like segregation conditions shall be defined. Hence, an automated routing method has been

proposed for topology generation of power supply systems in this paper. The proposed method has been applied to the electric power supply system for assessment.

To generate a system topology using the automated routing method, routing areas need to be defined. These routing areas can be defined based on areas within an aircraft where routing is typically performed. The defined routing areas are connected by pre-defined connection nodes, such as the intersection of the fuselage and the wing. With connecting all the routing areas, a single undirected graph is created, allowing to perform the shortest path routing between two components using Dijkstra's algorithm. To perform power segregation, components whose power supply shall be segregated need to be identified and assigned to a segregation group. As a next step, a cost function is added to the assigned paths for components of this group, artificially increasing the length of the paths.

It has been demonstrated that the automated routing method effectively generates the topology of the electric power supply system. This holds true for both the shortest path finding and the integration of a cost function as a boundary condition to perform power segregation for selected components. However, performing power segregation based on a cost function only ensures the selection of alternative paths. So far, it has not been differentiated if the alternative path is located nearby the shortest reference path. Therefore, a further parameter has to be integrated to assess the distance between the routing paths.

For future work, further evaluation criteria using the automated routing method need to be implemented. In the scope of this paper, the power segregation has been demonstrated and discussed as a boundary condition for the routing. In addition, further boundary conditions like the consideration of no-routing areas and the assessment of required and available installation space need to be implemented. Also, to be able to evaluate system integration aspects, the automated routing method needs to be applied for other supply systems, such as the hydraulic power supply system, the pneumatic power supply system, and the hydrogen supply system. In this case, further criteria like interdependencies and minimum distances between systems can be considered and evaluated.

Acknowledgements The results of the presented paper are part of the work in the research project development of systems and components for electrified flight (ESBEF), which is supported by the Federal Ministry of Economic Affairs and Climate Action in the national LuFo VI program. Any opinions, findings, and conclusions expressed in this document are those of the authors and do not necessarily reflect the views of the other project partners.

Funding Open Access funding enabled and organized by Projekt DEAL.

Data availability Data sets generated during the current study are available from the corresponding author on reasonable request. However, data sets containing aircraft geometries cannot be shared.

Declarations

Conflict of interest The authors have no relevant financial or non-financial interests to disclose.

Open Access This article is licensed under a Creative Commons Attribution 4.0 International License, which permits use, sharing, adaptation, distribution and reproduction in any medium or format, as long as you give appropriate credit to the original author(s) and the source, provide a link to the Creative Commons licence, and indicate if changes were made. The images or other third party material in this article are included in the article's Creative Commons licence, unless indicated otherwise in a credit line to the material. If material is not included in the article's Creative Commons licence and your intended use is not permitted by statutory regulation or exceeds the permitted use, you will need to obtain permission directly from the copyright holder. To view a copy of this licence, visit <http://creativecommons.org/licenses/by/4.0/>.

References

- Bielsky, T., Juenemann, M., Thielecke, F.: Parametric modeling of the aircraft electrical supply system for overall conceptual systems design. In: German Aerospace Congress, Aachen (2021). <https://doi.org/10.25967/530143>
- Juenemann, M., Thielecke, F., Peter, F., Hornung, M., Schülke, F., Stumpf, E.: Methodology for design and evaluation of more electric aircraft systems architectures within the avacon project. In: German Aerospace Congress, Darmstadt (2019). <https://doi.org/10.25967/480197>
- Kuelper, N., Broehan, J., Bielsky, T., Thielecke, F.: Systems architecting assistant (sara) - enabling a seamless process chain from requirements to overall systems design. In: 33rd Congress of the International Council of the Aeronautical Sciences, Stockholm, Sweden (2022)
- Juenemann, M., Kriewall, V., Bielsky, T., Thielecke, F.: Overall systems design method for evaluation of electro-hydraulic power supply concepts for modern mid-range aircraft. In: AIAA AVIATION Forum (2022). <https://doi.org/10.2514/6.2022-3953>
- Bielsky, T., Kuelper, N., Thielecke, F.: Overall parametric design and integration of on-board systems for a hydrogen-powered concept aircraft. In: Aerospace Europe Conference, Lausanne (2023)
- Zhu, Z., La Rocca, G., van Tooren, M.J.L.: A methodology to enable automatic 3d routing of aircraft electrical wiring interconnection system. CEAS Aeronaut. J. **8**(2), 287–302 (2017). <https://doi.org/10.1007/s13272-017-0238-3>
- Eisenhut, D., Moebs, N., Windels, E., Bergmann, D., Geiß, I., Reis, R., Strohmayer, A.: Aircraft requirements for sustainable regional aviation. Aerospace **8**(3), 61 (2021). <https://doi.org/10.3390/aerospace8030061>
- Garriga, A.G., Govindaraju, P., Ponnusamy, S.S., Cimmino, N., Mainini, L.: A modelling framework to support power architecture trade-off studies for more-electric aircraft. Transport. Res. Proc. **29**, 146–156 (2018). <https://doi.org/10.1016/j.trpro.2018.02.013>
- Alder, M., Moerland, E., Jepsen, J., Nagel, B.: Recent advances in establishing a common language for aircraft design with cpacs. In: Aerospace Europe Conference, Bordeaux (2020)
- Hause, M., Kihlström, L.-O.: You can't touch this! logical architectures in mbse and the uaf. In: 32nd Annual INCOSE International Symposium, Detroit (2022). <https://doi.org/10.1002/iis2.12941>
- Koeppen, C.: Methodik zur Modellbasierten Prognose Von Flugzeugsystemparametern Im Vorentwurf Von Verkehrsflugzeugen. Schriftenreihe Flugzeug-Systemtechnik. Shaker Verlag GmbH, Hamburg (2006)
- Fuchte, J., Nagel, B., Gollnick, V.: Automated fuselage system layout using knowledge based design rules. In: German Aerospace Congress, Berlin (2012)
- Moir, I., Seabridge, A.: Aircraft Systems: Mechanical, Electrical, and Avionics Subsystems Integration, Aerospace series, 3rd edn. Wiley, Chichester (2008)
- Pfennig, M.: Methodik zum Wissensbasierten Entwurf der Antriebssysteme Von Hochauftriebssystemen. Schriftenreihe Flugzeug-Systemtechnik. Shaker Verlag GmbH, Hamburg (2012)
- Van der Velden, C., Bil, C., Yu, X., Smith, A.: An intelligent system for automatic layout routing in aerospace design. Innov. Syst. Softw. Eng. **3**(2), 117–128 (2007). <https://doi.org/10.1007/s11334-007-0021-4>
- Coleman, T.F., Moré, J.J.: Estimation of sparse Jacobian matrices and graph coloring problems. SIAM J. Numer. Anal. **20**, 187–209 (1983)
- Diestel, R.: Graph Theory. Springer-Verlag GmbH, Berlin (2017). <https://doi.org/10.1007/978-3-662-53622-3>
- Lv, Z., Yang, L., He, Y., Liu, Z., Han, Z.: 3d environment modeling with height dimension reduction and path planning for uav. In: 9th International Conference on Modelling, Identification and Control (ICMIC), Kunming (2017). <https://doi.org/10.1109/ICMIC.2017.8321551>
- Hart, P., Nilsson, N., Raphael, B.: A formal basis for the heuristic determination of minimum cost paths. IEEE Trans. Syst. Sci. Cybern. **4**(2), 100–107 (1968). <https://doi.org/10.1109/TSSC.1968.300136>
- Cormen, T.H., Leiserson, C.E., Rivest, R.L., Stein, C.: Introduction to Algorithms. The MIT Press, Cambridge (2022)
- Dijkstra, E.W.: A note on two problems in connexion with graphs. Numer. Math. **1**(1), 269–271 (1959). <https://doi.org/10.1007/BF01386390>
- Schneegans, A.: Investigating systems architectures at the aircraft level-towards a holistic framework for the aircraft systems design process. In: German Aerospace Congress, Berlin (2012)
- Sarlioglu, B., Morris, C.T.: More electric aircraft: review, challenges, and opportunities for commercial transport aircraft. IEEE Trans. Transport. Electrification **1**(1), 54–64 (2015). <https://doi.org/10.1109/TTE.2015.2426499>
- A complete range of wire & cable solutions for aerospace applications Issue 9. Nexans, Draveil (2013)
- Schefer, H., Fauth, L., Kopp, T.H., Mallwitz, R., Friebe, J., Kurrat, M.: Discussion on electric power supply systems for all electric aircraft. IEEE Access **8**, 84188–84216 (2020). <https://doi.org/10.1109/ACCESS.2020.2991804>
- Nawawi, A., Simanjorang, R., Gajanayake, C.J., Gupta, A.K., Tong, C.F., Yin, S., Sakanova, A., Liu, Y., Liu, Y., Kai, M., See, K.Y., Tseng, K.-J.: Design and demonstration of high power density inverter for aircraft applications. IEEE Trans. Ind. Appl. **53**(2), 1168–1176 (2017). <https://doi.org/10.1109/TIA.2016.2623282>
- Huang, Z., Yang, T., Adhikari, J., Wang, C., Wang, Z., Bozhko, S., Wheeler, P.: Development of high-current solid-state power controllers for aircraft high-voltage dc network applications. IEEE Access **9**, 105048–105059 (2016). <https://doi.org/10.1109/ACCESS.2021.3099257>

Publisher's Note Springer Nature remains neutral with regard to jurisdictional claims in published maps and institutional affiliations.